SPECT- and Fluorescence Image–Guided Surgery Using a Dual-Labeled Carcinoembryonic Antigen–Targeting Antibody

Mark Rijpkema[1], Wim J. Oyen[1], Desiree Bos[1], Gerben M. Franssen[1], David M. Goldenberg[2,3], and Otto C. Boerman[1]

[1]Department of Radiology and Nuclear Medicine, Radboud University Medical Center, Nijmegen, The Netherlands; [2]Immunomedics, Inc., Morris Plains, New Jersey; and [3]Center for Molecular Medicine and Immunology, Garden State Cancer Center, Morris Plains, New Jersey

Intraoperative visualization techniques promise to significantly improve the detection and resection of tumors. In this study, we used an anti–carcinoembryonic antigen (CEA) antibody (MN-14) tagged with both a radiolabel (^{111}In) and a fluorophore (IRDye 800CW) for radionuclide detection and intraoperative fluorescence imaging, respectively. **Methods:** For this purpose, we prepared and characterized the dual-labeled antibody ^{111}In-diethylenetriaminepentaacetic acid (DTPA)-MN-14-IRDye 800CW and performed 4 studies on mice with subcutaneous and intraperitoneal CEA–expressing tumors: a dose escalation study to determine the optimal MN-14 protein dose, a biodistribution study comparing dual-labeled MN-14 and radiolabeled MN-14, a study to determine the optimal time for SPECT and fluorescence imaging after injection of dual-labeled MN-14, and finally a SPECT and fluorescence image–guided surgery study using this dual-labeled antibody. **Results:** The optimal protein dose of dual-labeled MN-14 was 10 μg per mouse, yielding a tumor-to-blood ratio of 3.5 within 72 h. The biodistribution of ^{111}In-DTPA-MN-14-IRDye 800CW in mice with subcutaneous LS174T tumors showed tumor uptake after 3 d (19.7% ± 17.0% injected dose/g) comparable to that of ^{111}In-DTPA-MN-14 but higher accumulation in the liver. The optimal time for imaging after administration of the dual-labeled antibody was 2–3 d after injection. Finally, in mice with intraperitoneally growing LS174T tumor nodules that received ^{111}In-DTPA-MN-14-IRDye 800CW, intraperitoneal tumor nodules could be localized with SPECT imaging after 3 d and subsequently resected using fluorescence image–guided surgery. **Conclusion:** Thus, we showed the feasibility for assessment and image-guided resection of CEA antigen–expressing tumors using dual-labeled MN-14. Both radionuclide detection and fluorescence imaging may provide useful information to improve localization of tumors and radical excision of tumor tissue. Because humanized MN-14 (labetuzumab) is available for clinical use, translation to a clinical setting is the next step.

Key Words: colorectal cancer; MN-14; CEA; fluorescence imaging; image-guided surgery

J Nucl Med 2014; 55:1519–1524
DOI: 10.2967/jnumed.114.142141

Received Apr. 24, 2014; revision accepted May 30, 2014.
For correspondence or reprints contact: Mark Rijpkema, Department of Nuclear Medicine 756, Radboud University Medical Center, P.O. Box 9101, 6500 HB Nijmegen, The Netherlands.
E-mail: mark.rijpkema@radboudumc.nl
Published online Jun. 30, 2014.

Colorectal cancer is the third most commonly diagnosed cancer in men and the second in women in the Western world, and the third most common cause of cancer deaths (*1*). Radical surgical resection of tumor tissue is the best or only chance for cure. However, surgical procedures may be complex and may involve multiple exenterative visceral resections requiring care by multiple specialists (*2*). Despite increasingly sophisticated surgery and adjuvant therapy, local recurrence is observed in up to 10% of colorectal cancer patients (*3*). Because the presence of microscopic residual tumor tissue at the resection margins is one of the main prognostic factors (*4*), optimizing the surgical procedure to prevent positive resection margins is of the utmost importance. Accordingly, intraoperative margin assessment and visualization techniques may be advantageous in guiding the surgeon to achieve curative resections.

During surgery, tumor localization and resection can be enhanced using specific radiotracers that target tumor tissue and can be detected by a γ probe (*5*). In addition to localizing primary tumors, radioguided surgery is commonly used for sentinel lymph node detection. Although this technique is extremely useful for localizing tumor-draining lymph nodes intraoperatively, it cannot precisely delineate the tumor. The addition of a fluorescent label could help overcome this limitation. Intraoperative fluorescence imaging could allow accurate real-time tumor delineation, but the penetration depth of emitted light in biologic tissue is limited to a few millimeters (*6*). Therefore, a powerful synergy can be achieved by combining radiotracers for the detection of tumor tissue and optical tracers for subsequent accurate delineation and resection of tumor lesions.

Although nontargeted approaches have proven valuable for sentinel lymph node mapping, these agents are not tumor-specific and hence not optimally suited for determination of the tumor-free margins (*7*). Also, distant metastases cannot be assessed using this approach. Tumors may be targeted using antibodies directed against tumor-associated antigens. Colorectal cancer can be targeted using the high-affinity monoclonal antibody (mAb) MN-14 (*8*) directed against the carcinoembryonic antigen (CEA). Both primary and metastatic colorectal cancer lesions show consistently high expression of this antigen (*9*). Radiolabeled MN-14 has been used as a tumor-targeting agent in both preclinical and clinical studies of colorectal cancer (*10–16*). Dual-modality intraoperative imaging in colon carcinoma patients may improve radical tumor resection, which has been shown to be directly related to patient

survival in peritoneally metastasized colorectal cancer (*17*). As the first step toward clinical application of dual-modality image-guided surgery, here we tagged MN-14 with both a radioactive (^{111}In) and a fluorescent (IRDye 800CW; LI-COR Biosciences) label and assessed biodistribution, SPECT and fluorescence imaging, and image-guided surgery using this dual-labeled antibody in mice with CEA-expressing tumors.

MATERIALS AND METHODS

Study Overview

In total, 4 studies were conducted with dual-labeled MN-14. First, a dose escalation study was performed to determine the optimal MN-14 protein dose in mice with subcutaneous CEA-expressing tumors. Using this optimal dose, in a second study the biodistribution of dual-labeled MN-14 and radiolabeled MN-14 without the fluorescent label was compared. Third, the optimal time for SPECT and fluorescence imaging after injection of dual-labeled MN-14 was determined. Finally, SPECT and subsequent fluorescence image–guided surgery were applied using dual-labeled MN-14.

Tumor Model

Female 6- to 8-wk-old athymic BALB/c *nu/nu* mice (Janvier) weighing 20–25 g were used in the experiment. The mice were allowed to become accustomed to laboratory conditions for at least 1 wk before the experiment started. The animals were housed in filter-topped cages under nonsterile standard conditions with free access to standard animal chow and water in accordance with institutional guidelines. Subcutaneous tumors (studies 1 and 2) were induced by subcutaneous injection in the right flank of 3×10^5 LS174T cells in 200 μL of RPMI 1640 medium. After 10–14 d, when the tumors reached a size of about 0.2 cm^3, the dual-labeled antibody preparations were administered intravenously. Intraperitoneal tumors (studies 3 and 4) were induced as described previously (*16*). In brief, mice were inoculated intraperitoneally with 10^6 LS174T cells suspended in 300 μL of RPMI 1640 medium. Experiments were continued 2 wk after tumor inoculation. All experiments were approved by the Animal Welfare Committee of the Radboud University Medical Center and were conducted in accordance with the Revised Dutch Act on Animal Experimentation (Wet op de Dierproeven).

Synthesis of Dual-Labeled MN-14

Murine MN-14, a high-affinity (association constant, 10^{-9} M) class III anti-CEA (CEACAM5) IgG1 antibody produced by a hybridoma cell line was provided by Immunomedics, Inc. (*18*). The antibody was conjugated with IRDye 800CW-NHS and SCN-Bz-diethylenetriaminepentaacetic acid (DTPA) in 2 steps. First, MN-14 (2 mg) was conjugated with IRDye 800CW-NHS in 350 μL of 0.1 M $NaHCO_3$, pH 8.5, with an 8-fold molar excess of IRDye 800CW-NHS. After 1.5 h of incubation at room temperature on an orbital shaker in the dark, the reaction mixture was purified by gel filtration using a PD-10 column (Amersham Biosciences) with 0.1 M $NaHCO_3$, pH 9.5, as eluent. Fractions with the highest protein concentration as determined spectrophotometrically were subsequently concentrated by centrifugal ultrafiltration (Amicon Ultra filter, molecular weight cutoff of 10,000; Millipore) to a volume of 350 μL. Second, SCN-Bz-DTPA (Macrocyclics) was added in a 12-fold molar excess. After 1 h of incubation at room temperature on an orbital shaker in the dark, the reaction mixture was dialyzed for 5 d in a Slide-A-Lyzer (10-kDa cutoff; Pierce Biotechnology Inc.) against 0.25 M NH_4Ac, pH 5.4. The final concentration of the mAb was determined spectrophotometrically at 280 nm (Ultrospec 2000 spectrophotometer; Pharmacia Biotech), correcting for absorption of the dye at that wavelength (3%, according to the manufacturer's protocol). The molar substitution ratio of the fluorescent dye was determined spectrophotometrically at 774 nm using a calibration curve of IRDye 800CW in phosphate-buffered saline (PBS).

Radiolabeling and Quality Control of the MN-14 Conjugate

For the biodistribution studies on mice with subcutaneous tumors, DTPA-MN-14-IRDye 800CW was radiolabeled with 0.1 MBq of ^{111}In (Covidien) per microgram of antibody in 0.1 M 2-(*N*-morpholino) ethanesulfonic acid (MES) buffer, pH 5.4 (3 times the volume of $^{111}InCl_3$ solution), and incubated for 30 min at room temperature under metal-free conditions. For the SPECT/CT studies, DTPA-MN-14-IRDye 800CW was radiolabeled with 3.9 MBq of ^{111}In per microgram of antibody under the same conditions. After incubation, 50 mM ethylenediamine tetraacetic acid solution was added (final concentration, 5 mM) to chelate unincorporated ^{111}In. The labeling efficiency was determined by instant thin-layer chromatography on silica gel strips (Agilent Technologies) using 0.15 M citrate buffer, pH 6.0, as the mobile phase. The labeling efficiency was greater than 95% for the biodistribution studies. For the SPECT/CT studies, ^{111}In-DTPA-MN-14-IRDye 800CW was purified by gel filtration using a PD-10 column with 0.5% bovine serum albumin in PBS as eluent, and the radiochemical purity of the final product was greater than 95% as determined by instant thin-layer chromatography. This dual-labeled MN-14 was used in studies 2–4.

For the dose escalation study (study 1), the fluorescently labeled antibody was radiolabeled with ^{125}I (instead of ^{111}In). Radioiodination was performed using the IODO-GEN method (*19*). In short, the antibody and ^{125}I were incubated at room temperature in 85 μL of PBS (0.10 M, pH 7.4) in a glass vial coated with 100 μg of IODO-GEN. After 10 min, the reaction was stopped by the addition of 100 μL of a saturated tyrosine solution. The labeling efficiency of all radioiodination reactions exceeded 70%. Subsequently, the ^{125}I-MN-14-IRDye 800CW was purified by gel filtration on a PD-10 column with 0.5% bovine serum albumin in PBS as eluent.

The immunoreactivity of the radiolabeled MN-14 preparations was determined using LS174T cells, as described by Lindmo et al. (*20*), with minor modifications. A serial dilution of LS174T cells was incubated with the MN-14 conjugate (10 μg/mL) for 30 min at 37°C. Subsequently, cells were centrifuged and washed with 500 μL of RPMI medium and analyzed in a γ counter (Wizard; Pharmacia-LKB). For all preparations, the immunoreactivity exceeded 70%.

Finally, the optical properties of both the IRDye 800CW and the DTPA-MN-14-IRDye 800CW were investigated. For this purpose, absorbance and fluorescence spectra of both samples in 50/50 serum/PBS were acquired using an Infinite M200 Pro multimode reader (Tecan).

Biodistribution

Biodistribution studies were performed by euthanizing the mice using O_2/CO_2 asphyxiation 1–8 d after injection of 200 μL of MN-14 conjugates. Subsequently, tumor, blood, muscle, lung, heart, spleen, pancreas, stomach, intestine, kidney, and liver were dissected and weighed. Activity was measured in a γ counter. To calculate the uptake of radiolabeled antibodies in each sample as a fraction of the injected dose, aliquots of the injected dose were counted simultaneously. The results were expressed as percentage injected dose (%ID) per gram.

SPECT and Fluorescence Imaging

SPECT/CT images were acquired using the U-SPECT-II/CT system (MILabs). Mice were scanned for 60 min using a 1.0-mm-diameter pinhole collimator tube, followed by a CT scan (spatial resolution, 160 μm; 65 kV; 612 μA) for anatomic reference. Scans were reconstructed with MILabs software, using an ordered-subset expectation maximization algorithm with a voxel size of 0.375 mm.

Fluorescence images were acquired using an in vivo imaging system (Xenogen VivoVision IVIS Lumina II; Caliper Life Sciences). The

acquisition time was 1–5 min with the following parameters: F/stop, 2; binning medium; field of view, C; excitation filter, 745 nm; emission filter, indocyanine green (810–885 nm). Correction for autofluorescence was performed using a second acquisition of 10 s with an excitation filter of 675 nm.

Studies Conducted

Dose Escalation. Mice with subcutaneous LS174T tumors in their right flank received ^{125}I-MN-14-IRDye 800CW (0.2 MBq per mouse) together with unlabeled MN-14 to adjust the antibody dose to 1, 3, 10, 30, or 100 μg/mouse (5 mice per group). The molar substitution ratio of fluorescent dye to antibody was 2.1:1. Three days after injection of the dual-labeled antibody, the mice were euthanized and the biodistribution of the radiolabel was determined to assess the optimal MN-14 dose.

Biodistribution. To compare the biodistribution of dual-labeled MN-14 with radiolabeled MN-14 (without the fluorescent label), mice with subcutaneous LS174T tumors received 10 μg of ^{111}In-DTPA-MN-14 or 10 μg of ^{111}In-DTPA-MN-14-IRDye 800CW (molar substitution ratio of fluorescent dye to antibody, 2.0:1; 1 MBq per mouse; 8 mice per group). Two mice from the ^{111}In-DTPA-MN-14 group also received 200 μg of unlabeled MN-14 (excess cold) to assess the specificity of the localization of the radiolabeled MN-14 conjugate. Three days after injection of antibodies, the mice were euthanized and biodistribution studies were performed.

Optimal Time for Imaging. Mice with intraperitoneally growing LS174T tumors received 10 μg of ^{111}In-DTPA-MN-14-IRDye 800CW (molar substitution ratio of fluorescent dye to antibody, 1.9:1; 40 MBq per mouse). After 1, 2, 3, or 8 d (5 mice at each time point), SPECT/CT imaging and fluorescence imaging were performed. Subsequently, the mice were euthanized and the biodistribution of the radiolabel was determined to assess the optimal time for imaging after administration of the antibody.

Preoperative SPECT and Fluorescence Image–Guided Surgery. Using the optimal settings as determined in the previous studies, finally a dual-modality image–guided surgery study was performed. Mice with intraperitoneally growing LS174T tumors received 10 μg of ^{111}In-DTPA-MN-14-IRDye 800CW (molar substitution ratio of fluorescent dye to antibody, 1.9:1; 39 MBq per mouse; 4 mice) or 10 μg of a dual-labeled anti-PSMA antibody that served as a negative control (^{111}In-DTPA-D2B-IRDye 800CW, molar substitution ratio of fluorescent dye to antibody, 1.8:1; 21 MBq per mouse; 4 mice). Three days after administration of the antibodies, preoperative SPECT/CT images were acquired, followed by fluorescence imaging of the mice in supine position after surgical relocation of skin, abdominal muscle layers, and peritoneum. Subsequently, the visualized tumor nodules were resected and fluorescence imaging was repeated to check for residual tumor tissue. This procedure was repeated until all visible tumor nodules were removed.

Statistical Analysis

All statistical analyses were performed using InStat, version 5.03 (GraphPad Software). Single comparisons were analyzed with 2-tailed, unpaired *t* tests. Statistical significance was set at a *P* level of less than 0.05.

RESULTS

The absorbance and fluorescence spectra of both the IRDye 800CW and the DTPA-MN-14-IRDye 800CW are shown in Figure 1. Similar patterns of fluorescence emission of the fluorophore before and after conjugation with the antibody were observed in the near-infrared region we used for fluorescence detection (810–885 nm).

In the first study on mice with subcutaneous LS174T tumors, the optimal MN-14 dose was determined in a dose escalation study. The tumor-to-blood ratio of mice that received 1, 3, 10, 30, or 100 μg of ^{125}I-MN-14-IRDye 800CW was 2.8, 3.2, 3.5, 3.0, and 2.9, respectively. On the basis of these results, a 10-μg dose of MN-14 was chosen as optimal in the subsequent studies.

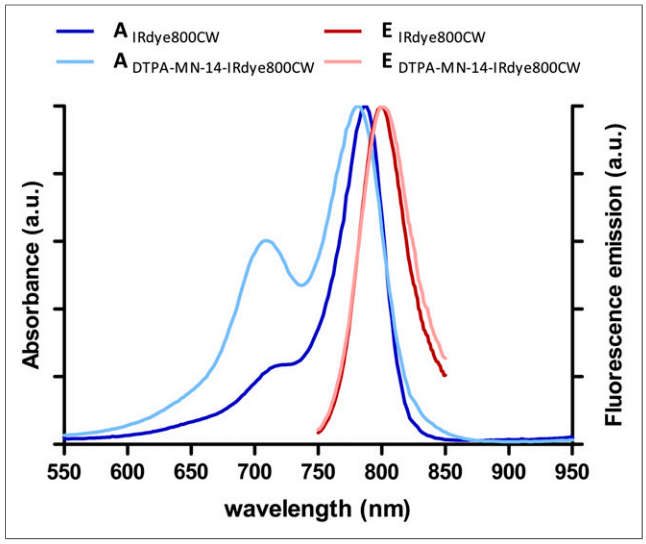

FIGURE 1. Absorption (A) and fluorescence emission (E) of IRDye 800CW and DTPA-MN-14-IRDye 800CW in 50/50 serum/PBS.

Next, the biodistribution of dual-labeled MN-14 was compared with the biodistribution of radiolabeled MN-14 (without the fluorescent label). The average weight of the tumors in this subcutaneous model was 0.58 ± 0.6 g and 0.58 ± 0.4 g for mice that received ^{111}In-DTPA-MN-14 or ^{111}In-DTPA-MN-14-IRDye 800CW, respectively. An example of the fluorescence imaging results is shown in Figure 2. The biodistribution results are summarized in Figure 3. The tumor uptake after 3 d was 26.4 ± 10.1 and 19.7 ± 17.0 %ID/g for ^{111}In-DTPA-MN-14 and ^{111}In-DTPA-MN-14-IRDye 800CW, respectively ($P = 0.44$). Compared with the radiolabeled MN-14, ^{111}In-DTPA-MN-14-IRDye 800CW showed higher accumulation in the liver (8.8 ± 0.8 vs. 18.6 ± 9.1 %ID/g, respectively, $P = 0.012$). Adding an excess of unlabeled MN-14 decreased tumor uptake to 10.7 ± 3.2 %ID/g and the tumor-to-blood level to 0.80 ± 0.18, showing that uptake of labeled MN-14 was specific.

FIGURE 2. Photograph (left) and fluorescence image (right) of mouse bearing subcutaneous CEA-expressing LS174T tumor 3 d after administration of ^{111}In-DTPA-MN-14-IRDye 800CW. sr = steradian.

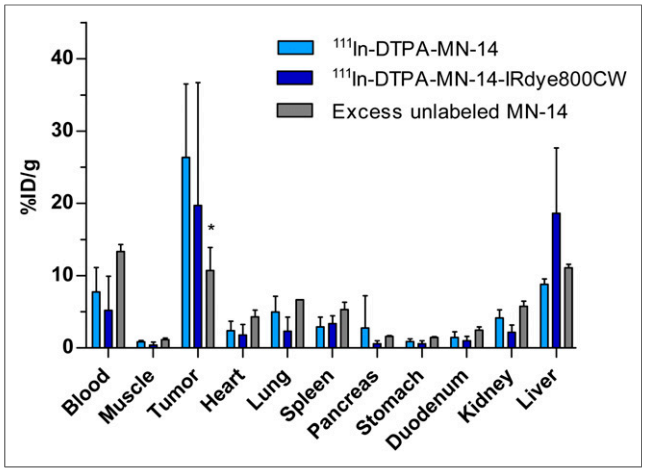

FIGURE 3. Biodistribution of dual-labeled MN-14 (dark blue) and radiolabeled MN-14 (light blue) in mice with subcutaneous LS174T tumors 3 d after administration of ^{111}In-DTPA-MN-14-IRDye 800CW or ^{111}In-DTPA-MN-14. Two mice from ^{111}In-DTPA-MN-14 group also received excess of unlabeled MN-14 (gray). *Tumor uptake $P < 0.05$.

In the third study, we determined the optimal time for imaging after administration of ^{111}In-DTPA-MN-14-IRDye 800CW. After 1, 2, 3, or 8 d, SPECT/CT imaging, fluorescence imaging, and biodistribution studies were performed. At each time point, tumors could be visualized with both SPECT and fluorescence imaging. Although absolute tumor uptake was highest on days 1 and 2 (10.9, 10.9, 7.9, and 5.1 %ID/g for days 1, 2, 3, and 8, respectively), tumor-to-liver ratios (0.39, 0.37, 0.46, and 0.38 for days 1, 2, 3, and 8, respectively) peaked on day 3. From this information, 2–3 d after administration of ^{111}In-DTPA-MN-14-IRDye 800CW was chosen as the optimal time point for imaging intraperitoneal tumors. From the blood values on days 1, 2, 3, and 8, we estimated the half-life of ^{111}In-DTPA-MN-14-IRDye 800CW to be 2.3 d.

Finally, we performed preoperative SPECT imaging and fluorescence image–guided surgery on mice bearing intraperitoneally growing tumors. First, SPECT images were acquired and fast reconstruction of the data using only the first iteration was performed to get a quick snapshot of the distribution of the radioactive label. Subsequently, mice were euthanized and laparotomy was performed to macroscopically search for intraperitoneal tumors. When suspected tumors were found on the basis of SPECT imaging results and visual inspection, fluorescence imaging was applied and tumors were surgically removed. Figure 4 shows the SPECT and fluorescence images of a mouse that received ^{111}In-DTPA-MN-14-IRDye 800CW. The SPECT images clearly show 2 larger tumor nodules in the left upper abdomen and multiple smaller ones in the right abdominal region. Visual inspection and fluorescence imaging visualized the 2 larger tumor nodules, and these were subsequently resected (Fig. 4).

In total, 13 intraperitoneal tumors were resected from the 4 mice in this group. The average weight of these tumors was 0.02 g. The weight of the tumors in 2 mice was too small to be determined accurately. These tumor nodules were excluded from further analysis. Ex vivo analyses indicated a tumor uptake of 29.5 ± 2.2 %ID/g and a tumor-to-liver ratio of 5.4 ± 1.2, which was marginally higher than the tumor-to-liver ratio found in the subcutaneous model (tumor-to-liver ratio, 2.2 ± 2.5; $P = 0.070$).

Mice that received the control dual-labeled antibody ^{111}In-DTPA-D2B-IRDye 800CW did not show any specific accumulation of the tracer in the tumor on either SPECT or fluorescence images (data not shown). This finding was confirmed by the biodistribution results (tumor: 3.4 ± 0.7 %ID/g; blood: 6.9 ± 0.4 %ID/g).

DISCUSSION

In this study, we showed the feasibility of image-guided surgery using dual-labeled MN-14 in CEA-expressing tumor models. We found high and specific accumulation of the dual-labeled antibody in CEA-expressing tumors and a good correlation between the radiosignal and the fluorescent signal. Furthermore, intraoperative fluorescence imaging was shown to provide surgical guidance for the resection of intraperitoneally growing tumors. However, very small tumor nodules (<0.02 g) that were deeper in the peritoneal cavity could be detected only on the basis of the radiosignal of the dual-labeled antibody, underlining the limitation of fluorescence imaging and the importance of a dual-mode approach. We also showed that the pharmacokinetics of fluorescently labeled antibodies may change compared with unlabeled antibodies, leading to faster blood clearance, increased liver accumulation, and decreased tumor uptake. This finding has been reported for other fluorescently labeled antibodies as well and has been attributed to conformational changes to the antibody due to conjugation of the fluorophore (*21*) but may also be explained by the lipophilicity and negative charge of the fluorophore, which may lead to increased albumin binding (*22*) and subsequent liver uptake.

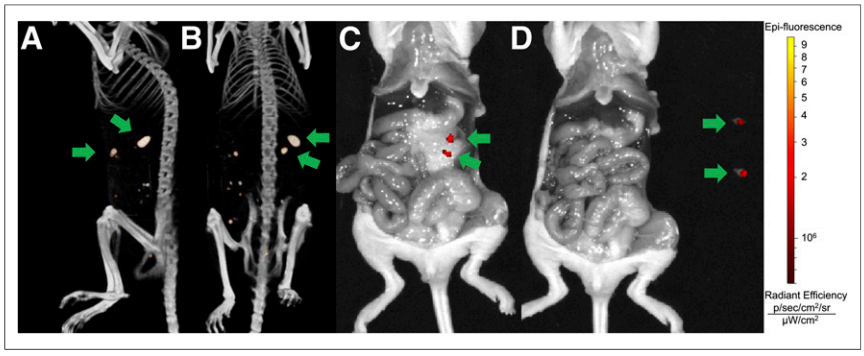

FIGURE 4. SPECT/CT images (lateral [A] and supine [B] positions) of mouse bearing intraperitoneal CEA-expressing tumors 3 d after administration of ^{111}In-DTPA-MN-14-IRDye 800CW. Laparotomic inspection using fluorescence imaging revealed 2 visible tumor nodules, as indicated by arrows (C), that were subsequently removed using fluorescence-guided surgery (D). sr = steradian.

The specific uptake of MN-14 in CEA-expressing tumors as observed in our study has been reported before and has led to a series of studies using radiolabeled MN-14 for imaging and radioimmunotherapy of CEA-positive tumors (*23*). In these studies, an increased median survival of mice with subcutaneous or intraperitoneal tumors was found after radioimmunotherapy with radiolabeled MN-14, and the therapeutic efficacy of the high-affinity mAb MN-14 was shown to be superior to low-affinity anti-CEA mAbs (*10,13,16,23*). In addition to MN-14, other anti-CEA mAbs also have been used in preclinical studies. For example, a green fluorophore-labeled anti-CEA

antibody was shown to improve tumor detection and resection in open laparotomies in mouse models (*24,25*), and recurrence rates were significantly decreased in mice after fluorescence-guided surgery (*26*).

Clinically, anti-CEA antibodies have been used in both imaging and therapy studies of several types of cancer (*27–32*). Radiolabeled MN-14 has been used in clinical studies mainly for radioimmunotherapy, and encouraging results have been shown both in colorectal cancer (*10,12,33*) and in medullary thyroid carcinoma (*28,34*). Although radiolabeled anti-CEA antibodies have shown their potential in the clinic for SPECT imaging and radioimmunotherapy, image-guided surgery has not been performed yet with these tracers. For this purpose, the combination of both a radiolabel and a fluorescent label for detection and accurate resection of tumors could be advantageous. After intravenous injection of such a probe, primary tumor, lymph nodes, and distant metastases may be assessed by preoperative noninvasive whole-body PET or SPECT imaging, which can contribute to decisions on therapeutic management (e.g., whether to perform laparotomy). However, the main application of dual-modality imaging is the option for subsequent intraoperative tumor disclosure. During surgery, tumor localization may be improved using intraoperative scintillation detection, followed by fluorescence imaging to facilitate radical tumor resection. Preclinically, this approach has shown promising results in mice with human xenografts with antivascular endothelial growth factor antibodies and antihuman epidermal growth factor 2 antibodies labeled with ^{89}Zr and the fluorescent dye IRDye 800CW (*35*). Recently, Zhang (*36*) and Hong (*37*) showed the feasibility of this approach in CD105-expressing breast tumor xenografts using dual-labeled TRC105.

Patients with peritoneal carcinomatosis of colorectal origin may particularly benefit from image-guided surgery using dual-labeled MN-14, as these patients may be eligible for cytoreductive surgery followed by hyperthermic intraperitoneal chemotherapy (*38*). It has been shown that the extent of cytoreduction has a direct impact on survival, and maximal cytoreduction is one of the most powerful determinants for survival among peritoneal carcinomatosis patients (*17*). Because the tumor lesions in these patients may be small and numerous, and tumor tissue may not be easily discriminated from normal or scar tissue, surgical outcome in these patients may be improved by image-guided surgery.

CONCLUSION

Targeted intraoperative fluorescence imaging has been demonstrated in ovarian cancer patients and may revolutionize oncologic surgery (*39*). Here, we have shown the feasibility and potential of this method in CEA-expressing tumors using MN-14 in colorectal cancer xenografts. Furthermore, we extended this technique by using a dual-labeled probe, enabling both preoperative and intraoperative radiodetection and subsequent fluorescence imagegguided surgery. This result now requires clinical translation.

DISCLOSURE

The costs of publication of this article were defrayed in part by the payment of page charges. Therefore, and solely to indicate this fact, this article is hereby marked “advertisement” in accordance with 18 USC section 1734. Dr. Goldenberg is employed by and has stock in Immunomedics, Inc., which has patented and owns the MN-14 antibody used in this study. No other potential conflict of interest relevant to this article was reported.

ACKNOWLEDGMENTS

We thank Bianca Lemmers-van de Weem, Henk Arnts, Iris Lamers-Elemans, and Kitty Lemmens-Hermans for their technical assistance with the animal experiments.

REFERENCES

1. Jemal A, Bray F, Center MM, Ferlay J, Ward E, Forman D. Global cancer statistics. *CA Cancer J Clin.* 2011;61:69–90.
2. Beyond TME Collaborative. Consensus statement on the multidisciplinary management of patients with recurrent and primary rectal cancer beyond total mesorectal excision planes. *Br J Surg.* 2013;100:E1–E33.
3. Sjövall A, Granath F, Cedermark B, Glimelius B, Holm T. Loco-regional recurrence from colon cancer: a population-based study. *Ann Surg Oncol.* 2007; 14:432–440.
4. Nagtegaal ID, Quirke P. What is the role for the circumferential margin in the modern treatment of rectal cancer? *J Clin Oncol.* 2008;26:303–312.
5. Povoski SP, Neff RL, Mojzisik CM, et al. A comprehensive overview of radioguided surgery using gamma detection probe technology. *World J Surg Oncol.* 2009;7:11.
6. Luker GD, Luker KE. Optical imaging: current applications and future directions. *J Nucl Med.* 2008;49:1–4.
7. Keereweer S, Kerrebijn JD, van Driel PB, et al. Optical image-guided surgery: where do we stand? *Mol Imaging Biol.* 2011;13:199–207.
8. Sharkey RM, Goldenberg DM, Murthy S, et al. Clinical evaluation of tumor targeting with a high-affinity, anticarcinoembryonic-antigen-specific, murine monoclonal antibody, MN-14. *Cancer.* 1993;71:2082–2096.
9. Hammarström S. The carcinoembryonic antigen (CEA) family: structures, suggested functions and expression in normal and malignant tissues. *Semin Cancer Biol.* 1999;9:67–81.
10. Behr TM, Salib AL, Liersch T, et al. Radioimmunotherapy of small volume disease of colorectal cancer metastatic to the liver: preclinical evaluation in comparison to standard chemotherapy and initial results of a phase I clinical study. *Clin Cancer Res.* 1999;5:3232s–3242s.
11. Behr TM, Sharkey RM, Sgouros G, et al. Overcoming the nephrotoxicity of radiometal-labeled immunoconjugates: improved cancer therapy administered to a nude mouse model in relation to the internal radiation dosimetry. *Cancer.* 1997;80:2591–2610.
12. Hajjar G, Sharkey RM, Burton J, et al. Phase I radioimmunotherapy trial with iodine-131–labeled humanized MN-14 anti-carcinoembryonic antigen monoclonal antibody in patients with metastatic gastrointestinal and colorectal cancer. *Clin Colorectal Cancer.* 2002;2:31–42.
13. Koppe MJ, Bleichrodt RP, Soede AC, et al. Biodistribution and therapeutic efficacy of $^{125/131}$I-, ^{186}Re-, $^{88/90}$Y-, or ^{177}Lu-labeled monoclonal antibody MN-14 to carcinoembryonic antigen in mice with small peritoneal metastases of colorectal origin. *J Nucl Med.* 2004;45:1224–1232.
14. Koppe MJ, Oyen WJ, Bleichrodt RP, et al. Combination therapy using the cyclooxygenase-2 inhibitor Parecoxib and radioimmunotherapy in nude mice with small peritoneal metastases of colonic origin. *Cancer Immunol Immunother.* 2006;55:47–55.
15. Koppe MJ, Oyen WJ, Bleichrodt RP, Verhofstad AA, Goldenberg DM, Boerman OC. Combination therapy using gemcitabine and radioimmunotherapy in nude mice with small peritoneal metastases of colonic origin. *Cancer Biother Radiopharm.* 2006;21:506–514.
16. Koppe MJ, Soede AC, Pels W, et al. Experimental radioimmunotherapy of small peritoneal metastases of colorectal origin. *Int J Cancer.* 2003;106:965–972.
17. Glockzin G, Schlitt HJ, Piso P. Peritoneal carcinomatosis: patients selection, perioperative complications and quality of life related to cytoreductive surgery and hyperthermic intraperitoneal chemotherapy. *World J Surg Oncol.* 2009;7:5.
18. Hansen HJ, Goldenberg DM, Newman ES, Grebenau R, Sharkey RM. Characterization of second-generation monoclonal antibodies against carcinoembryonic antigen. *Cancer.* 1993;71:3478–3485.
19. Fraker PJ, Speck JC Jr. Protein and cell membrane iodinations with a sparingly soluble chloroamide, 1,3,4,6-tetrachloro-3a,6a-diphenylglycoluril. 1978. *Biochem Biophys Res Commun.* 2012;425:510–518.
20. Lindmo T, Boven E, Cuttitta F, Fedorko J, Bunn PA Jr. Determination of the immunoreactive fraction of radiolabeled monoclonal antibodies by linear extrapolation to binding at infinite antigen excess. *J Immunol Methods.* 1984;72:77–89.
21. Cohen R, Stammes MA, de Roos IH, Stigter-van Walsum M, Visser GW, van Dongen GA. Inert coupling of IRDye800CW to monoclonal antibodies for clinical optical imaging of tumor targets. *EJNMMI Res.* 2011;1:31.
22. Valko K, Nunhuck S, Bevan C, Abraham MH, Reynolds DP. Fast gradient HPLC method to determine compounds binding to human serum albumin: relationships

with octanol/water and immobilized artificial membrane lipophilicity. *J Pharm Sci.* 2003;92:2236–2248.
23. Blumenthal RD, Sharkey RM, Haywood L, et al. Targeted therapy of athymic mice bearing GW-39 human colonic cancer micrometastases with ^{131}I-labeled monoclonal antibodies. *Cancer Res.* 1992;52:6036–6044.
24. Kaushal S, McElroy MK, Luiken GA, et al. Fluorophore-conjugated anti-CEA antibody for the intraoperative imaging of pancreatic and colorectal cancer. *J Gastrointest Surg.* 2008;12:1938–1950.
25. Tran Cao HS, Kaushal S, Metildi CA, et al. Tumor-specific fluorescence antibody imaging enables accurate staging laparoscopy in an orthotopic model of pancreatic cancer. *Hepatogastroenterology.* 2012;59:1994–1999.
26. Metildi CA, Kaushal S, Luiken GA, Talamini MA, Hoffman RM, Bouvet M. Fluorescently labeled chimeric anti-CEA antibody improves detection and resection of human colon cancer in a patient-derived orthotopic xenograft (PDOX) nude mouse model. *J Surg Oncol.* 2014;109:451–458.
27. Behr TM, Becker WS, Klein MW, Bair HJ, Scheele JR, Wolf FG. Diagnostic accuracy and tumor-targeting kinetics of complete versus fragmented ^{99m}Tc-labeled anti-carcinoembryonic antigen antibodies: an intraindividual comparison. *Cancer Res.* 1995;55:5786s–5793s.
28. Juweid ME, Hajjar G, Swayne LC, et al. Phase I/II trial of ^{131}I-MN-14F(ab)2 anti-carcinoembryonic antigen monoclonal antibody in the treatment of patients with metastatic medullary thyroid carcinoma. *Cancer.* 1999;85:1828–1842.
29. Fuster D, Maurel J, Muxi A, et al. Is there a role for ^{99m}Tc-anti-CEA monoclonal antibody imaging in the diagnosis of recurrent colorectal carcinoma? *Q J Nucl Med.* 2003;47:109–115.
30. Yao YF, Yang Z, Li ZF, Gu J. Immunoscintigraphy of local recurrent rectal cancer with ^{99m}Tc-labeled anti-CEA monoclonal antibody CL58. *World J Gastroenterol.* 2007;13:1841–1846.
31. Takeda A, Shimada H, Okazumi S, et al. Preclinical assessment and pilot study using anti-CEA monoclonal antibody 1B2 for colorectal carcinoma imaging. *Hepatogastroenterology.* 2008;55:2054–2058.
32. Artiko V, Petrovic M, Sobic-Saranovic D, et al. Radioimmunoscintigraphy of colorectal carcinomas with ^{99m}Tc-labelled antibodies. *Hepatogastroenterology.* 2011;58:347–351.
33. Juweid M, Sharkey RM, Swayne LC, Griffiths GL, Dunn R, Goldenberg DM. Pharmacokinetics, dosimetry and toxicity of rhenium-188-labeled anti-carcinoembryonic antigen monoclonal antibody, MN-14, in gastrointestinal cancer. *J Nucl Med.* 1998;39:34–42.
34. Juweid M, Sharkey RM, Behr T, et al. Radioimmunotherapy of medullary thyroid cancer with iodine-131-labeled anti-CEA antibodies. *J Nucl Med.* 1996; 37:905–911.
35. Terwisscha van Scheltinga AG, van Dam GM, Nagengast WB, et al. Intraoperative near-infrared fluorescence tumor imaging with vascular endothelial growth factor and human epidermal growth factor receptor 2 targeting antibodies. *J Nucl Med.* 2011;52:1778–1785.
36. Zhang Y, Hong H, Severin GW, et al. ImmunoPET and near-infrared fluorescence imaging of CD105 expression using a monoclonal antibody dual-labeled with ^{89}Zr and IRDye 800CW. *Am J Transl Res.* 2012;4:333–346.
37. Hong H, Zhang Y, Severin GW, et al. Multimodality imaging of breast cancer experimental lung metastasis with bioluminescence and a monoclonal antibody dual-labeled with ^{89}Zr and IRDye 800CW. *Mol Pharm.* 2012;9:2339–2349.
38. Koppe MJ, Boerman OC, Oyen WJ, Bleichrodt RP. Peritoneal carcinomatosis of colorectal origin: incidence and current treatment strategies. *Ann Surg.* 2006;243:212–222.
39. van Dam GM, Themelis G, Crane LM, et al. Intraoperative tumor-specific fluorescence imaging in ovarian cancer by folate receptor-alpha targeting: first in-human results. *Nat Med.* 2011;17:1315–1319.